

Effect of annealing on structural and optical properties of indium sulfide thin layers produced by chemical bath deposition method

M Nasiri Sarvi¹, P Esmaili^{2*} and S Asgary³

¹School of New Technologies, Iran University of Science and Technology (IUST), Narmak, Tehran 16846, Iran

²Young Researchers and Elite Club, Islamic Azad University, Urmia Branch, Urmia, Iran

³Department of Physics, West Tehran Branch, Islamic Azad University, Tehran, Iran

Received: 22 February 2019 / Accepted: 26 July 2019 / Published online: 29 October 2019

Abstract: Indium sulfide thin films were prepared by chemical bath deposition method on glass substrates for about 40 min as deposition time and 60 °C as deposition temperature. The films were post-annealed at different temperatures such as 100 °C, 200 °C, 300 °C and 400 °C, for about 1 h. Structural and optical properties of In₂S₃ thin films after post-annealing process have been investigated. The crystallinity and nanostructures of the films were studied by using X-ray diffraction, scanning electron microscopy, energy-dispersive X-ray spectroscopy and atomic force microscopy analysis. Optical reflectance and transmittance of layers were measured in the wavelength of 300–1100 nm by spectrophotometer instrument. Kramers–Kronig relations were used to calculate the optical constants. The X-ray diffraction measurements showed transformation of an amorphous nature to a crystalline structure by increasing the annealing temperature. The atomic force microscopy images showed by increasing the annealing temperature, the roughness of the thin films increased. The scanning electron microscopy images revealed that growth rate increased consistently with the increase in annealing temperature and well-dispersed quasi-spherical nanoparticles with high agglomeration rate are formed at 400 °C. The energy-dispersive X-ray spectroscopy results show reduction in the S/In ratio from 1.61 to 1.49 when annealing temperature increased. Optical results showed the highest optical band gap of 3.65 eV was achieved at the highest annealing temperature (400 °C).

Keywords: Indium sulfide; Optical properties; Structural properties; Kramers–Kronig relations

PACS Nos.: 78.20.–e

1. Introduction

Indium sulfide (In₂S₃) is an III–VI semiconductor material with an n-type electrical conductivity. This semiconductor has a direct and large band gap that can be varied from 2 to 3.25 eV [1–3] by the addition of some elements such as oxygen or Na. Because of its good photoconductive properties, high transparency in the visible spectral region and chemical stability, In₂S₃ was appeared to be suitable to use in photovoltaic industries, optoelectronic and photoelectron chemical solar cell devices [4]. The electrical and optical properties of a β-In₂S₃ single crystal are stable at normal temperatures, and its band gap energy is about 1.98 eV [5].

In₂S₃ can exist in several polymorphs; thus, it is expected that the physical properties of In₂S₃ films significantly are dependent on the preparation conditions.

In₂S₃ thin films have been prepared by different methods such as physical vapor deposition (PVD), photochemical deposition (PCD) technique [6], spray pyrolysis [7], atomic layer epitaxy [8], atomic layer deposition [9], reactive evaporation [10], ionic layer gas atomic reaction (ILGAR), thermal evaporation [11, 12], modulated flux deposition [13] and chemical bath deposition (CBD) [14]. Chemical bath deposition is a promising method to deposit semiconductor films, such as CdS and In₂S₃, on different substrates at low temperature [15]. CBD has unique advantages such as low temperature deposition and uniform and stoichiometric films over large areas. CBD is also a useful and effective method that can be easily scaled up.

*Corresponding author, E-mail: parisa.esmail2018@gmail.com

In this study, effects of post-deposition annealing on deposited In_2S_3 thin films by CBD method were studied. The structural and optical properties of prepared thin films were systematically investigated as a function of annealing temperature.

The material properties can be enhanced by annealing processes. Post-annealing process causes improvement in the film's crystallinity and increases the grain size. Therefore, annealing of the films at optimized conditions could improve the film's quality with reduced surface roughness and defects present in the films [16]. In fact, the values of surface roughness and grain size can be controlled by adjusting the annealing temperature.

By studying the reflectance spectra of the deposited films on solid surfaces, optical constants (real and imaginary part of refractive indexes n and k) can be determined [17]. There are many different methods for determining the optical constants of materials. One of the most common techniques that have been used to determine the optical constants over the whole measurement range is Kramers–Kronig analysis [18].

The deposited films have been characterized by different techniques such as X-ray diffraction (XRD), scanning electron microscopy (SEM), energy-dispersive X-ray spectroscopy (EDS), atomic force microscopy (AFM) and optical spectra by spectrophotometry. (The optical parameters are calculated by Kramers–Kronig relations.)

Deposition conditions significantly have effect on the physical properties of In_2S_3 films. These results could help in controlling the structural parameters according to suitable morphological properties requirements for photovoltaic and other applications.

2. Experimental details

In_2S_3 thin films were prepared by CBD method on glass substrates. Prior to deposition, all glass substrates were ultrasonically cleaned in acetone and then ethanol. Aqueous solution containing thioacetamide (TA) and indium chloride (InCl_3) was used as sources of S_{2-} and In_{3+} , respectively, and acetic acid was used as complex agent of the In_{3+} . The resulting solution was diluted to 100 mL with water distilled. Deposition parameters were: $[\text{InCl}_3] = 25 \text{ mM}$; $[\text{TA}] = 350 \text{ mM}$; acid acetic = 300 mM. During the deposition, the bath temperature was constant at 70 °C and deposition time was 45 min. After deposition, the films were annealed at different temperatures such as 100 °C, 200 °C, 300 °C and 400 °C under vacuum for about 1 h. Phase structure of the deposited In_2S_3 films was identified using an X-Ray X' pert MPD diffractometer ($\text{CuK}\alpha$ radiation, $\lambda = 0.15406 \text{ nm}$) in the range of 10° to 80° with step size of 0.02. Nanostructures were investigated by SEM

(S-3400, Hitachi, Japan). Surface physical morphology was obtained by means of AFM (Dual Scope TM DS, 95-200/50). Reflectance of the films was determined with UV–Vis spectrophotometer (Hitachi, U-3310) instrument. Kramers–Kronig relations were derived to calculate optical properties such as α , n , k and optical band gap energy.

3. Results and discussion

3.1. Structural analysis

3.1.1. X-ray diffraction analysis

Figure 1 shows the XRD patterns of as-grown and annealed In_2S_3 films at different annealing temperatures such as 100 °C, 200 °C, 300 °C and 400 °C, respectively. In_2S_3 crystallizes in three phases, namely α , β and γ . The γ - In_2S_3 phase is stable at temperatures above 754 °C, α - In_2S_3 phase is stable at temperatures between 420 and 754 °C while β - In_2S_3 is stable at temperatures below 420 °C [19]. β - In_2S_3 crystal is a defect spinel lattice with a large number of vacancies [20], which can be seen as a quasi-ternary compound consisting of S, In and vacancies.

It is seen that the as-grown film has an amorphous structure. No characteristic peaks show up in the XRD patterns of the as-deposited samples. It is due to the low thermal energy, which is insufficient for significant crystallization [21].

Diffractogram of as-deposited In_2S_3 thin film depicts amorphous nature even after annealing at 100 °C and

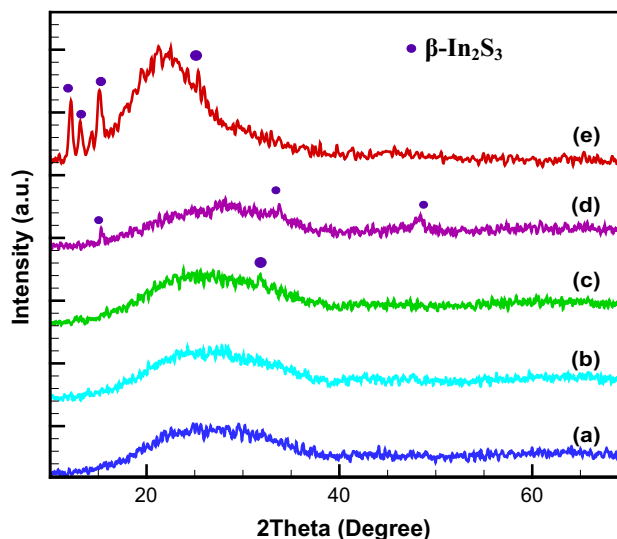


Fig. 1 XRD patterns of In_2S_3 thin films produced by CBD method at different annealing temperatures: (a) as deposited, (b) 100 °C, (c) 200 °C, (d) 300 °C and (e) 400 °C

crystalline structures at 200 °C, 300 °C and 400 °C under vacuum.

For the annealed sample at 200 °C, the crystallization begins. The amorphous structure transforms to crystalline structure which indicates the arrangement of atoms into volume. X-ray diffraction pattern shows a low-intensity peak at $2\theta = 31.78^\circ$ related to the (300) crystalline plane of the tetragonal In_2S_3 phase.

According to X-ray diffraction pattern for the annealed film at 300 °C, few minor peaks are observed at $2\theta = 15.23^\circ$, 33.75° and 48.33° that are related to the (101), (220) and (440) orientations, respectively, corresponding to tetragonal $\beta\text{-In}_2\text{S}_3$.

The crystallization is more evidence for the annealed film at 400 °C. The new peaks obtained at $2\theta = 12.08^\circ$, 13.51° , 15.09° and 25.21° are corresponding to crystallographic orientations of (111), (103), (101) and (109), respectively, which are related to tetragonal $\beta\text{-In}_2\text{S}_3$ phase (JCPDS: 73-1366) with (101) plane as its preferred orientation.

It seems that the intensity of X-ray diffraction peaks increases with annealing temperature. This may be due to thermal energy increase enough for crystallization and the grain growth.

3.1.2. Energy-dispersive X-ray spectroscopy

The elemental analysis of as-grown and annealed In_2S_3 thin films was carried out by employing energy-dispersive spectroscopy (EDS). The EDS analysis revealed that the annealing temperature had a significant influence on the stoichiometry of the grown films (Fig. 2). The data showed the presence of In and S elements and other impurity elements.

All films were nearly stoichiometric, and the S/In ratio decreased from 1.61 to 1.49 (bulk In_2S_3) with the increase in annealing temperature. The presence of Si and O elements in all samples was a sign of glass substrates in our experiments. The S/In ratio of annealed sample at 400 °C shows that the film is sulfur-deficient. The strongly decreasing sulfur content is due to its high volatility. In fact, the improvement in crystallinity of this film could be attributed to a rapid reaction of S vapor with In which would lead to $\beta\text{-In}_2\text{S}_3$ phase.

The post-annealing process carried out in vacuum is leading to additional loss of sulfur due to re-evaporation from the film [22, 23].

3.1.3. Scanning electron microscopy analysis

Figure 3 shows scanning electron microscopy of In_2S_3 on glass thin films produced by CBD method at different annealing temperatures such as 100 °C, 200 °C, 300 °C

and 400 °C, respectively. As shown in Fig. 3(a), nucleation sites of the In_2S_3 grains were observed. After 1-h annealing, small grains are visible on the surface of the film. By increasing the annealing temperature to 200 °C and 300 °C (shown in Fig. 3(b, c)) and increasing the ion energy, nucleation increased and grain growth occurred. Small spherical nanoparticles were coalescence and clusters formed. At 400 °C annealing temperature (Fig. 3(d)), there was a noticeable increase in the grain size. At this temperature, in addition to the nucleation and growth, coalescence and re-nucleation appear which has led to the formation of cavities.

3.1.4. Atomic force microscopy analysis

AFM data provide a high-magnification three-dimensional image of a solid surface and can examine the film morphology, roughness and grain size.

Figure 4 shows atomic force microscopy images of In_2S_3 on glass thin films at different annealing temperatures such as 100 °C, 200 °C, 300 °C and 400 °C, respectively. The as-deposited In_2S_3 thin films are continuous and homogeneous and show a slight roughness. It is observed from the images that the average height of the roughness profile increases with annealing temperature because of correlation between smaller particles.

However, in the case of the annealed films at different temperatures, the surface had a completely different morphology. The films annealed at higher temperature have a granular surface morphology. The morphology became coarser, and the height of distribution has changed when the annealing temperature was increased. It can be seen that the surface roughness increases with the increase in annealing temperature. The average roughness of as-deposited thin films was ~ 1.8 nm, but after annealing at 400 °C, the average roughness increased to ~ 4.19 nm. It seems due to aggregations of smaller crystallites.

4. Optical properties

It is common knowledge that the Kramers–Kronig relations connect real and imaginary parts of an analytic function describing some causal physical processes [23, 24]:

The complex reflectivity r in polar form is given by:

$$r(\omega) = R^{1/2}(\omega)e^{i\theta(\omega)}, \quad (1)$$

where R is the normal incidence reflectance and θ is the phase angle, which at energy E_0 can be calculated rigorously from the Kramers–Kronig integral:

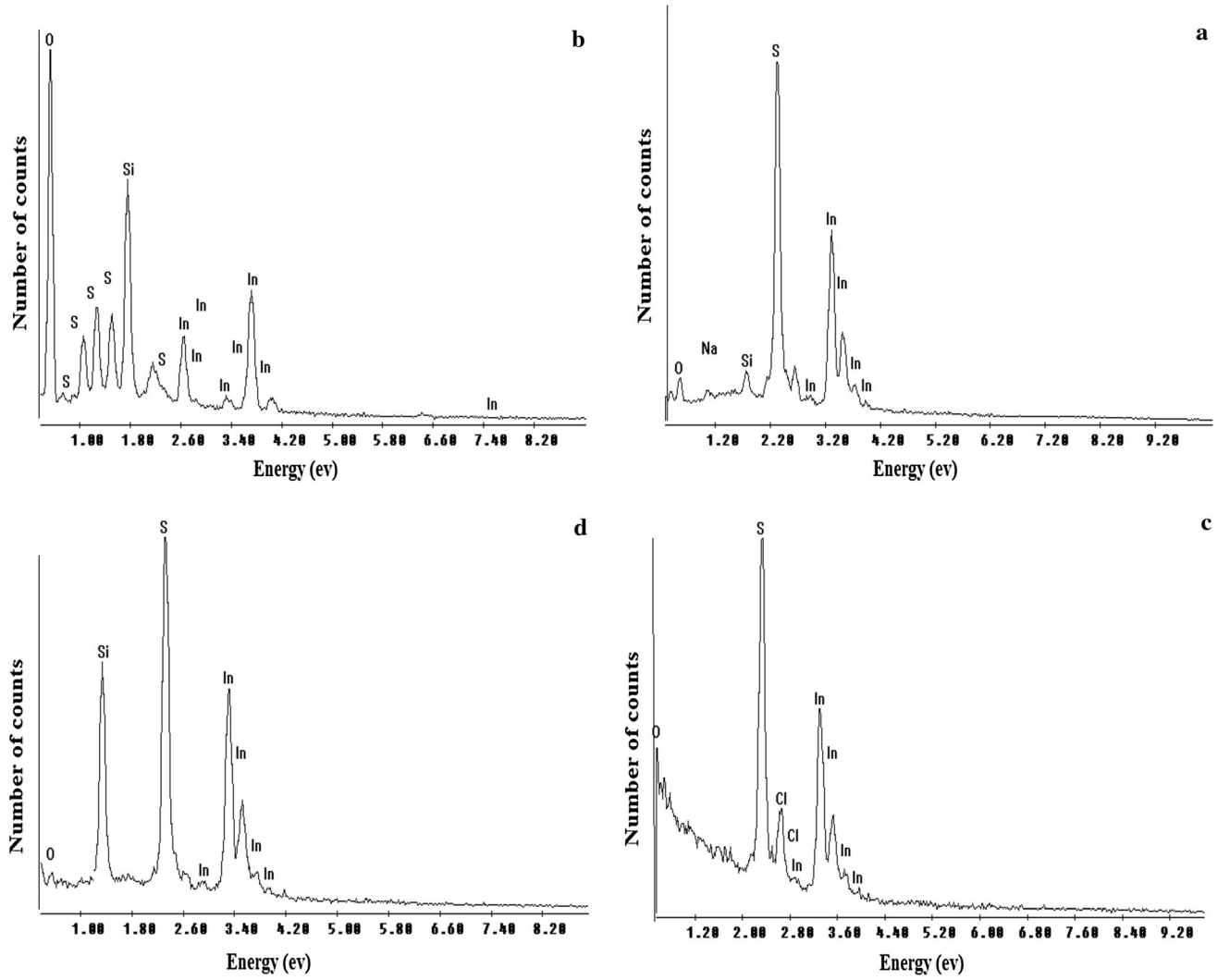


Fig. 2 EDS images of In_2S_3 on glass thin films produced by CBD method at different annealing temperatures: (a) 100 °C, (b) 200, (c) 300 °C and (d) 400 °C

$$\theta(E) = \frac{E}{\pi} \int_0^{E_2} \frac{L_n R(E) - L_n R(E_0)}{E^2 - E_0^2} dE, \quad (2)$$

where E is the photon energy, provided that the reflectance $R(E)$ is known for all energies. However, since R is not known over the entire energy range, it is necessary to extrapolate $R(E)$ to infinite energies, usually by a power law. One can use an extrapolation which will force the optical or dielectric constants to agree with some independent measurements at a particular energy. For example, ellipsometric measurements on metals will yield ε_1 , ε_2 or n , k directly. In order to calculate $\theta(\omega)$ from Eq. (2), the following procedure can be adopted. At very low energies, we assume that the reflectance at zero energy approaches unity. At high energies, when the incident photon energy is higher than certain energy E_2 , the

reflectance is determined from free electron asymptotic limit [25]:

$$R(E) = R(E_2) \times \left(\frac{E_2}{E}\right)^4 \quad (3)$$

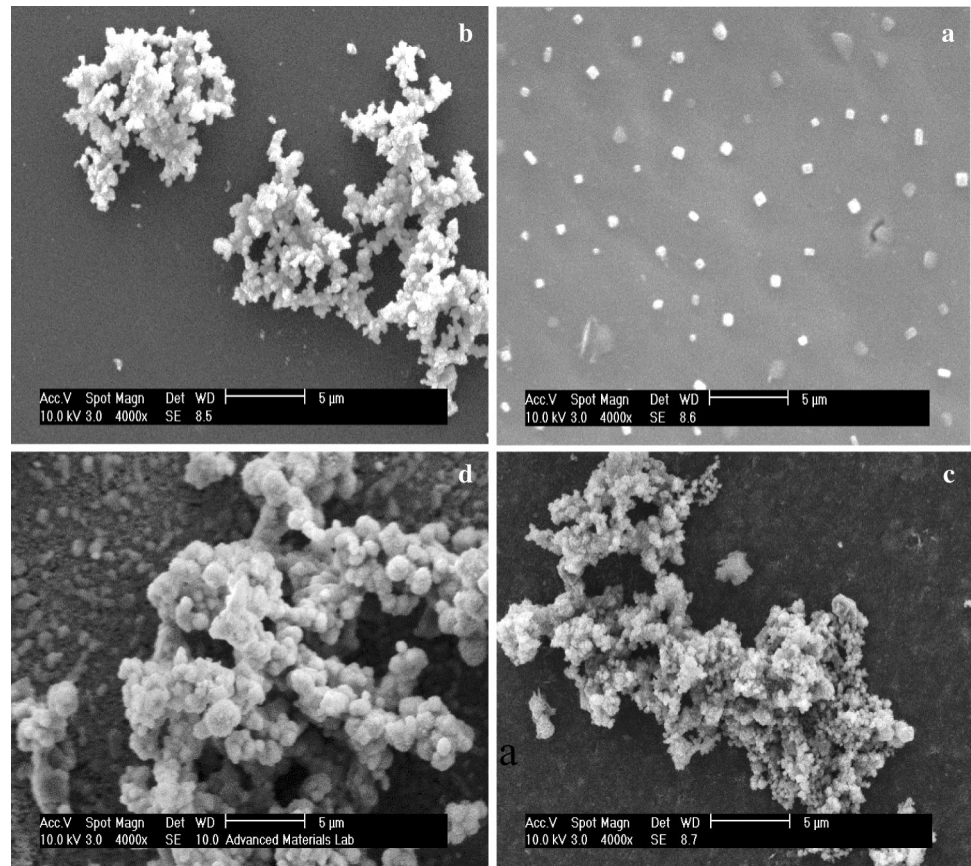
$$E > E_2$$

Substituting Eq. (2) in K-K Eq. (3), we have:

$$\begin{aligned} \theta(E) = & -\frac{E}{\pi} \int_0^{E_2} \frac{\ln R(E) - \ln R(E_0)}{E^2 - E_0^2} dE \\ & + \frac{1}{2\pi} \ln \left[\frac{R(E)}{R(E_2)} \right] \ln \frac{E_2 + E}{|E_2 - E|} \\ & + \frac{1}{\pi} \sum_{n=0}^{\infty} \left[4 \left(\frac{E}{E_2} \right)^{2n+1} \right] (2n+1) \end{aligned} \quad (4)$$

Hence, if E_2 is known, the $\theta(E)$ can be calculated. If the film thickness is taken as a known parameter, then for

Fig. 3 Scanning electron microscopy of In_2S_3 on glass thin films produced by CBD method at different annealing temperatures: (a) 100 °C, (b) 200, (c) 300 °C and (d) 400 °C



calculation of the real and the imaginary parts of the reflective index of the thin film (n_2 , k_2), two equations at one frequency are required. By substituting the known values of $\theta(E)$ and $R(E)$ in Eq. (1), the reflectance index $r(E)$ can also be determined with reference to the reflectance equation for a thin film [23] as:

$$r = \frac{r_{12} + r_{23}e^{2i\delta_2} + r_{31}e^{2i(\delta_2+\delta_3)} + r_{12}r_{23}r_{31}e^{2i\delta_3}}{1 + r_{12}r_{23}e^{2i\delta_2} + r_{12}r_{31}e^{2i(\delta_2+\delta_3)} + r_{23}r_{31}e^{2i\delta_3}}, \quad (5)$$

where r_1 , r_{23} , r_{31} , r_{12} , r_{23} and r_{31} are Fresnel reflectance indices [24] for air film, film–substrate and substrate–air boundaries and d_2 and d_3 are the film and the substrate thicknesses, respectively. In the case of normal incidence, we have:

$$R^{1/2}(E)_{\text{exp}} \cos \theta(E)_{\text{exp}} - R_e[r(n_2(E), k_2(E), d_2)] = 0 \quad (6)$$

$$R^{1/2}(E)_{\text{exp}} \sin \theta(E)_{\text{exp}} - I_m[r(n_2(E), k_2(E), d_2)] = 0 \quad (7)$$

The complex refractive index of any layer is written as $n_- = n + ik$ (8)

Here, the real part n is the refractive index and specifies the phase velocity, while the imaginary part κ is called the extinction coefficient or mass attenuation coefficient that

shows the amount of attenuation when the electromagnetic wave propagates through the material.

When the real and imaginary parts of the refractive index are determined, one can calculate the other optical constants. The results for optical properties are as follows:

Figure 5(a) shows the reflectance curves of In_2S_3 films deposited on glass substrates at different annealing temperatures such as 100 °C, 200 °C, 300 °C and 400 °C. As it can be seen, the increase in annealing temperature completely affects the reflectance spectra. It is seen that by increasing the annealing temperature, reflectance decreases. That is because of the formation of voids by increasing the annealing temperature. Experimental absorption coefficient is given as:

$$\alpha = \frac{2E}{hc}k(E) \quad (9)$$

where c is the velocity of light and $k(E)$ is the imaginary part of refractive index.

The absorbance coefficient curves of indium sulfide films annealed at different temperatures are shown in Fig. 5(b). With the increase in annealing temperature, transmittance increases and absorbance decreased. This decrease is because of the formation of more voids on the films. The lowest absorbance coefficient belongs to film

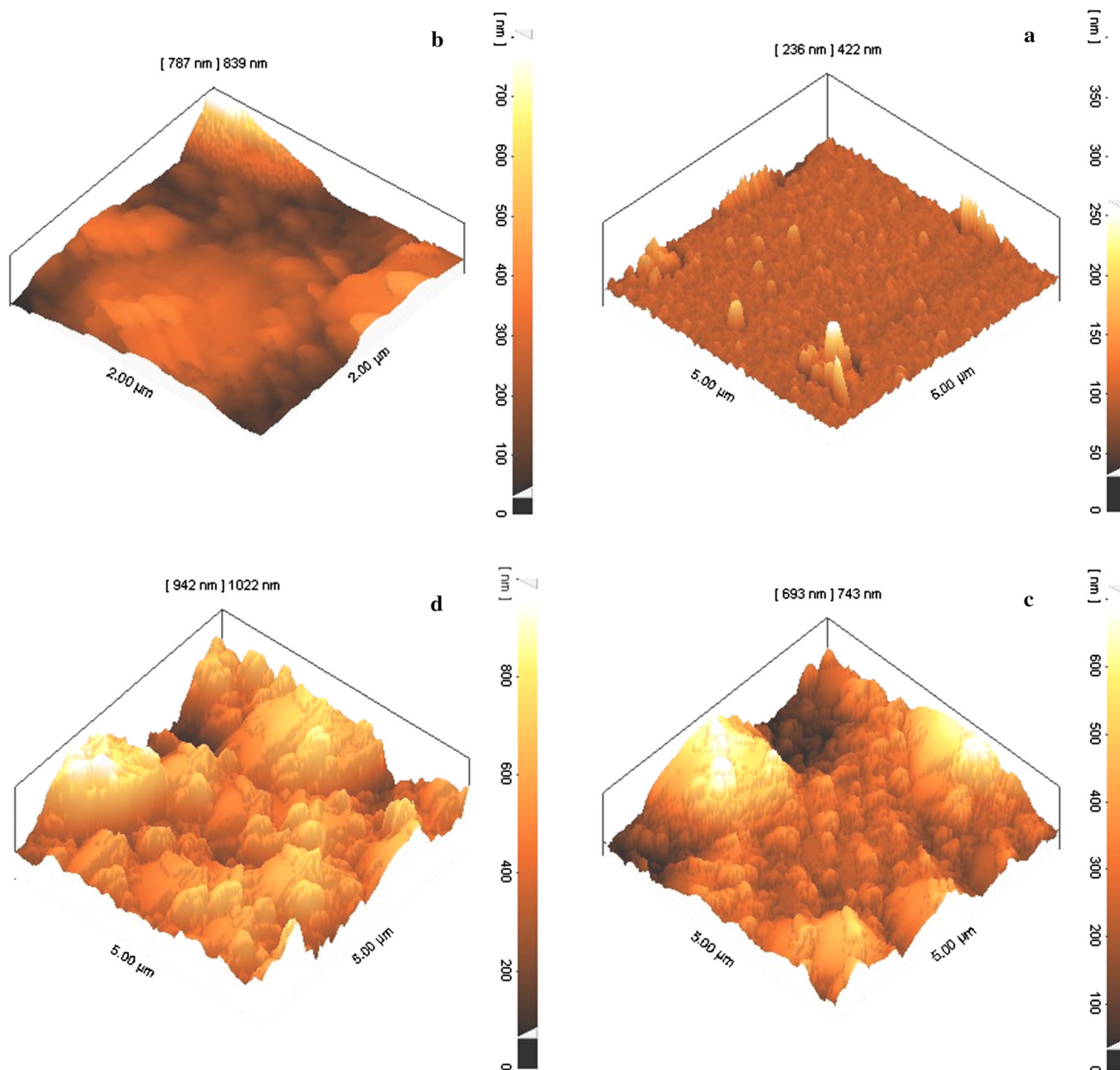


Fig. 4 Atomic force microscopy images of In_2S_3 on glass thin films produced by CBD method at different temperatures: (a) 100 °C, (b) 200, (c) 300 °C and (d) 400 °C

that annealed at 400 °C temperature. Figure 6(a) shows real part of refractive index (n), for In_2S_3 thin films at different annealing temperatures and other same deposition conditions. Here different curves correspond to different annealing temperatures. General trend of all curves is the same. By increasing the annealing temperature and formation of porous layers, real part of refractive index (n) decreased. In Fig. 6(b), we depict the imaginary part of refractive index (k), for In_2S_3 thin layers of different annealing temperatures. By increasing the annealing temperature, the surface of the layers becomes full of void

fractions so a rough surface appears which leads to a decreasing trend for the imaginary part of refractive index.

Figure 7 illustrates calculations of the optical band gap energy (E_g) for the layers in this work, which has been obtained by:

$$\alpha = (h\nu - E_g)^m \quad (10)$$

where ν is the frequency, E_g is the optical band gap and m ($= 2$) is a constant. The optical band gaps calculated for annealed samples at different temperatures are shown in Table 1.

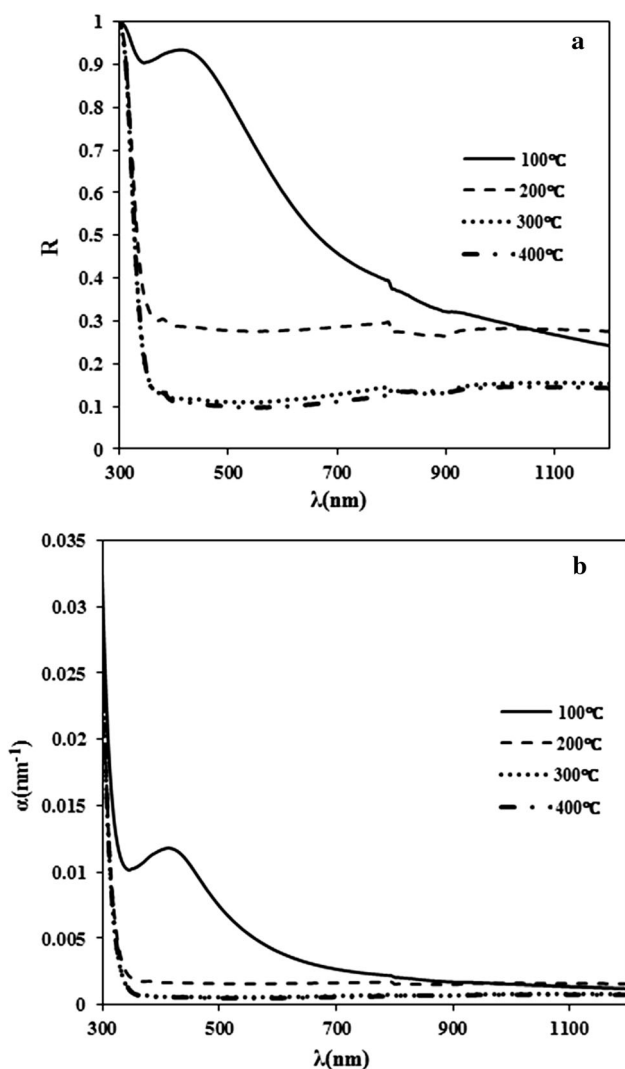


Fig. 5 Reflectance for In_2S_3 layers with different annealing temperatures

Increasing the annealing temperature leads to the increase in band gap energy that means more semiconductor films are produced. The increase in the optical band gap shows that the conductivity decreases with the increase in annealing temperature.

It is believed that the increase in band gap energy can contribute to the scattering [26].

It is also dependent on the morphology of the nanostructures [27].

It is found that the crystalline film was rougher than the amorphous film because of its grain growth at higher annealing temperature. The surface roughness causes reduction in mean free path lengths of scattered electrons [28].

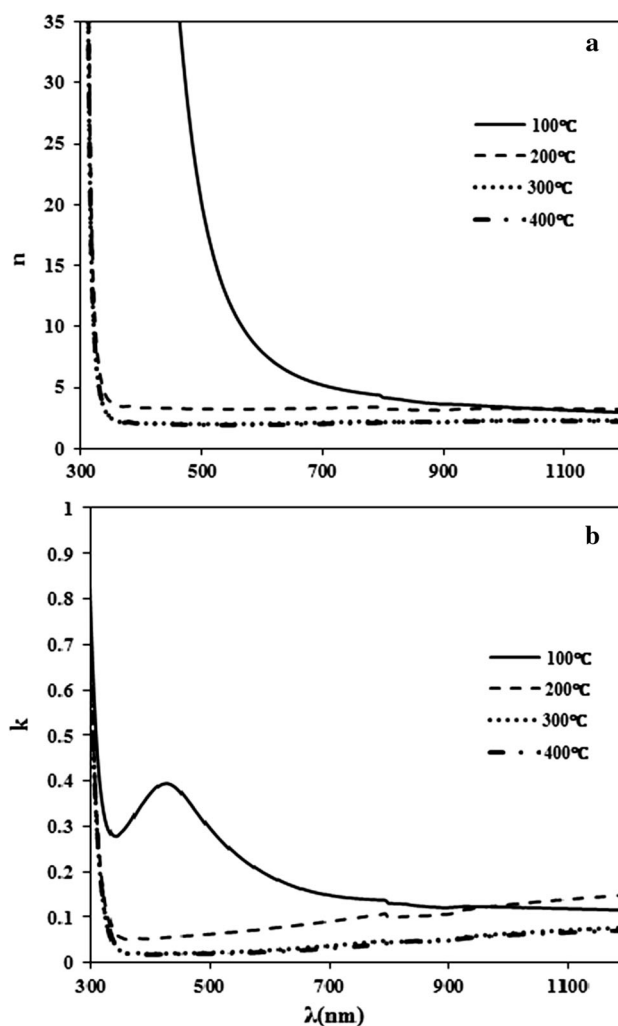


Fig. 6 Real part of refractive index for In_2S_3 layers with different annealing temperatures

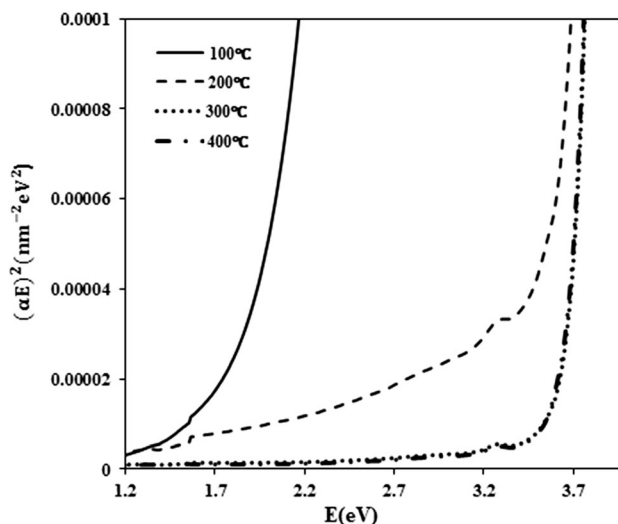


Fig. 7 Band gap energy of In_2S_3 layers with different annealing temperatures

Table 1 Values of band gap energies

In ₂ S ₃ /glass	Annealing temperature	Band gap energy (eV)
I	100	1.9
II	200	3.2
III	300	3.6
V	400	3.65

5. Conclusion

In this work, thin In₂S₃ films on glass substrates were prepared by chemical bath deposition (CBD) method, at different annealing temperatures such as 100 °C, 200 °C, 300 °C and 400 °C for about 60 min. The influence of annealing temperature on structural and optical properties and the relation between nanostructures and optical properties of In₂S₃ thin layers were investigated.

The XRD spectrums revealed that the films are amorphous in nature and exhibited improved crystallinity with tetragonal structure after annealing. The SEM images showed good uniformity and enhanced grain size with the increase in annealing temperature.

Morphology of films was changed by increasing the annealing temperature. RMS roughness of layers was increased by increasing the annealing temperature. The lower S/In ratio at higher annealing temperature (400 °C) shows that the film is sulfur-deficient, resulting from the evaporation of sulfur from the film.

The optical parameters of produced films were calculated by Kramers–Kronig relations on reflectivity curves in UV–Vis light wavelength range and correspondence energy range. By increasing the annealing temperature, reflectance decreases because of the formation of undesirable voids under deposition conditions. Optical band gap energy increases by increasing the annealing temperature that means more semiconductor films are produced.

References

- [1] J George, K S Joseph, B Pradeep, T I Palson *Phys. Stat. Sol. A* **106** 123 (1988)

- [2] E B Yousfi, T Asikainen, V Pietu, P Cowache, M Powlla, D Lincot *Thin Solid Films* **361** 183 (2000)
- [3] N Barreau, J C Bernede, S Marsillac *J. Cryst. Growth* **241** 51 (2002)
- [4] M I Hossain *Chalcogenide Lett.* **9** 185 (2012)
- [5] M Ichimura, A Nakamura, K Takenchi, E Arai *Thin Solid Films* **384** 157 (2001)
- [6] R Kumareasan, M Ichimura, N Stato, P Ramasamy *Mater. Sci. Eng. B Solid-State Mater. Adv. Technol.* **96** 37 (2002)
- [7] N Kamoun, R Bennaceur, M Amlouk, S Belgacem, N Mliki, J M Frigerio, M C Theye *Phys. Status Solidi A Appl. Res.* **169** 97 (1998)
- [8] N Bouguila, H Bouzouita, E Lacaze, A BelHadj Amara, H Bouchriha, A Dhouib *J. Physique III* **7** 1647 (1997)
- [9] N Naghavi, R Henriquez, V Laptev, D Lincot *Appl. Surf. Sci.* **222** 65 (2004)
- [10] T Asikainen, M Ritila, M Leskela *Appl. Surf. Sci.* **82/83** 122 (1994)
- [11] J George, K S Joseph, B Pradeep, T I Palson *Phys. Status Solidi A Appl. Res.* **106** 123 (1988)
- [12] A A Elshazly, D Abdelkady, H S Metoually, M A M. Segman *J. Phys. Condens. Mater.* **10** 5943 (1998)
- [13] C Guille'an, T Garico, J Herrero, M T Gutierrez, F Briones *Thin Solid Films* **112** 451 (2004)
- [14] J H Kim, D Shin, B T Ahn *Curr. Appl. Phys.* **16** 1040 (2016)
- [15] H Kangarlou, M Motallebi Agh Gonbad, A Abdollahi *Mater. Sci. Semicond. Process.* **1** 1 (2015)
- [16] S Rasool, K Saritha, K T Ramakrishna Reddy, M S Tivanov, A V Trofimova, S E Tikoto, L Bychto, A Patryn, M Maliński, V F Gremenok *Curr. Appl. Phys.* **11** 16 (2018)
- [17] O A Castelo-González, H C Santacruz-Ortega, M A Quevedo-Lo'pez M Sotelo-Lerma *J. Electr. Mater.* **41** 695 (2012)
- [18] E Jalili, H Kangarlou, P Esmaili *Optik* **127** 11235 (2016)
- [19] D Diehl, R Nitsche *J. Crystal Growth* **20** 38 (1973)
- [20] K S J B M Kambas *Phys. Status Solidi (b)* **105** 291 (1981)
- [21] M T Bhatti, A M Rana, A F Khan *Mater. Chem. Phys.* **84** 126 (2004)
- [22] E Li ta, J E Sanchez *J. Appl. Phys.* **85** 876 (1999)
- [23] G B Arfken, H J Weber *Mathematical methods for physics* (Port Harcourt: Harcourt Science and Technology Company) (2001)
- [24] E D Palik *Handbook of optical constants of solids* (Cambridge: Courtesy Academic Press Inc) (1985)
- [25] L Ward *The optical constants of bulk materials and films* (Philadelphia: Institute of Physics) (1988)
- [26] C C Ting, S Y Chen *J. Appl. Phys.* **88** 4628 (2000)
- [27] G Zhang, K Lu, X Zhang, W Yuan, M Shi, H Ning, R Tao, X Liu, R Yao, *J. Peng Micromachines* **9** 377 (2018)
- [28] S. Asgary, M. Hantehzadeh, M. Ghoranneviss, A. Boochani *Rare Metals* **40** 1 (2016)

Publisher's Note Springer Nature remains neutral with regard to jurisdictional claims in published maps and institutional affiliations.